


Article

A Novel Continuously Variable Transmission with Circumferentially Arranged Disks (CAD CVT)

Muhammad Bilal¹, Qidan Zhu^{1,*}, Shafiq R. Qureshi^{2,3}, Ahsan Elahi¹, Muhammad Kashif Nadeem² and Sartaj Khan² 

- ¹ College of Intelligent Systems, Science and Engineering, Harbin Engineering University, Harbin 150001, China; muhammadbilal@hrbeu.edu.cn or muhammadbilalemenust@gmail.com (M.B.); ahsan.elahi@hrbeu.edu.cn (A.E.)
- ² Centers of Excellence in Science and Applied Technologies (CESAT), Islamabad P.O. Box 2801, Pakistan; shafique@pnec.nust.edu.pk or shafiqpn1@hotmail.com (S.R.Q.); mkn3ch@gmail.com (M.K.N.); sartaj.physics@gmail.com (S.K.)
- ³ Pakistan Navy Engineering College, National University of Sciences and Technology (NUST), Karachi 44000, Pakistan
- * Correspondence: zhuqidan@hrbeu.edu.cn

Abstract: This paper presents a novel Continuous Variable Transmission (CVT) design. CVT is highly beneficial for actuators with rotary output as it can improve the energy efficiency of the actuators by providing an optimum transmission ratio. This property of CVT is highly beneficial for fossil-fuel-based vehicles, electric vehicles, wind turbines, industrial robots, etc. With the exception of Spherical CVT and DH CVT, all known CVTs like push belt CVTs, toroidal CVTs, Milner CVTs, etc., require additional gear sets and clutches for direction reversal and neutral gear ratio. However, Spherical CVT and DH CVT have low torque capacity due to a single traction point constraint. Foregoing in view, a new CVT named CAD CVT has been developed. The paper presents the design conception, the operating principle, the transmission ratio, the torque capacity, frictional losses, and experimental verification of the basic functionality by manufacturing a Proof of Concept (PoC). The proposed CVT is the only CVT capable of independent direction reversal and high torque capacity as it can transmit torque through multiple traction points. The new CVT will significantly impact high-torque applications in different engineering applications, especially land transport consisting of heavy vehicles like trucks, buses, and trailers.

Keywords: continuous variable transmission (CVT); multi traction; high torque; negative gear ratios; direction reversal; truck CVT



Citation: Bilal, M.; Zhu, Q.; Qureshi, S.R.; Elahi, A.; Nadeem, M.K.; Khan, S. A Novel Continuously Variable Transmission with Circumferentially Arranged Disks (CAD CVT). *Actuators* **2024**, *13*, 208. <https://doi.org/10.3390/act13060208>

Academic Editor: Dong Jiang

Received: 26 March 2024

Revised: 19 May 2024

Accepted: 23 May 2024

Published: 3 June 2024



Copyright: © 2024 by the authors. Licensee MDPI, Basel, Switzerland. This article is an open access article distributed under the terms and conditions of the Creative Commons Attribution (CC BY) license (<https://creativecommons.org/licenses/by/4.0/>).

1. Introduction

Continuous Variable Transmission (CVT) is a device that can provide infinite gear ratios between two finite limits. Therefore, it can provide optimum gear ratios for transmission and thus improve the energy efficiency of IC engines [1], pure electric vehicles [2], hybrid electric vehicles [3], hybrid hydraulic excavators [4], wind turbines [5,6], mobile robots [7], or any other robotic application [8]. In addition to energy efficiency, traction-based CVT can not only improve the back drivability of robots but can also improve the inherent force-limiting capabilities of robotic systems in a human–robot interactive environment [9,10].

Due to the various advantages, applications, and uses of CVTs, several CVTs have been developed. Notable variations of CVTs include traction-based CVTs, belt and chain-based CVTs, and ratcheting-type CVTs.

Most of the CVTs designed so far are traction-based. Chen et al. [11] developed a type of traction CVT named wheel-type CVT (W-CVT), which has a complex gear system and more traction contacts in series as compared to a toroidal CVT. Kazerounian et al. [12]

developed a parallel disk continuous variable transmission (PD CVT), which has low torque capacity. Komatsubara et al. [13] designed a cone-to-cone CVT (CTC CVT), which also has low torque capacity. Carter et al. [14] developed motion CVT, which is quite similar to the Kopp Variator and has some positive attributes, like ease of manufacturing, lightweight, and compactness. Shen et al. [15] designed a hydraulic traction drive CVT, which comprises a speed-regulating mechanism, one input disc, one output disc, four inner rollers, and four outer rollers with better efficiency and power capacity. Ghariblu et al. [16] developed a ball-type CVT (B CVT), which has a simple structure, and its efficiency is comparable to a toroidal CVT. Traction-based CVTs are prone to spin losses. The spin losses can only be eliminated when the axes of rotation of the driving and the driven elements and tangent to the contact area between the driving and driven elements either intersect at a single point or are parallel. The second condition is not possible in a CVT. However, the first condition can be achieved. Li et al. [17] effectively applied the intersecting condition to a Toroidal CVT by proposing a Logarithmic generatrix. The new CVT showed higher efficiency but resulted in a reduced transmission range and a significant increase in the complexity of the controlling mechanism. Chao et al. [18] developed a no-spin CVT (NS CVT). The no-spin capability was achieved by remodeling the original generatrix to achieve the intersecting condition of no-spin. NS CVT was compared with half-toroidal CVT and it was observed that NS CVT has better efficiency but a lower torque. Chao et al. [19] developed a new configuration synthesis method called the configuration factor table method (CFT Method). Application of the CFT method to logarithmic CVT and conical CVT resulted in fourteen variants of logarithmic CVT and ten variants of conical CVT. Out of these, rolling logarithmic CVT, swing logarithmic CVT, rolling conical CVT, and swing conical CVT may emerge as the new generation. Delkhosh et al. [20] optimized the geometry of full toroidal CVT so that its efficiency can be increased and mass can be reduced. NuVinci drive is a type of CVT that closely resembles the Kopp Variator. Tomaselle et al. [21] analyzed the Nu Vinci drive and concluded that slight adjustments in geometry can improve the efficiency. Verbelen et al. [22] analyzed half-toroidal CVT and concluded that an increase in clamping force improves the dynamics of CVT but degrades its efficiency. Toroidal CVT is an important type of CVT, which can be classified into full-toroidal and half-toroidal CVT. Carbone et al. [1] analyzed and compared half-toroidal and full-toroidal CVT and observed that for most of the region, half-toroidal has better efficiency and torque transmission.

Belt-type CVTs are the most common type of CVTs. Different variations of the belt-type CVTs have been developed and analyzed like the steel-pushing V belt CVT [23], DAR CVT [24], and DBV CVT [23]. One problem with belt-type CVTs is that to increase torque capacity, the clamping force also has to be increased, which results in reduced efficiency [24]. There is an emerging class of CVTs in which a linear reciprocating motion is changed to a unidirectional rotary motion through one-way clutches. The cam-based CVT developed by Patil et al. [25] and the ratcheting-type CVT developed by Olyaei [26] are a few examples. These CVTs are prone to vibration and energy losses due to the reciprocating motion of internal masses.

All the CVTs mentioned above [11–28] have one major problem. They require an additional gear set and clutches for direction reversal and neutral gear ratio.

So far, only the DH CVT [29] and spherical CVT [30] can achieve directional reversal and neutral gear ratio independently. The major problem with the DH CVT [29] and spherical CVT [30] is that a single traction point constraint severely limits their torque capacity.

Our literature survey indicates that there is currently no CVT capable of providing both high torque and the ability to reverse its direction while also achieving neutral gear ratios without the need for an additional gear set and clutches. Hence, it is vital to engineer a novel CVT that can achieve direction reversal and a neutral gear ratio without the need for an additional gear set or clutches. Moreover, the suggested CVT will have the capability to transmit torque across several traction points, allowing it to be specifically designed for high-torque applications such as trucks.

In this research, a novel CVT has been designed. The CVT has been named the circumferentially arranged disks CVT (CAD CVT). The unique feature of the CVT is that it can achieve direction reversal and a neutral gear ratio without requiring an additional gear set and clutches. Moreover, it can be designed for any amount of torque by increasing the traction points. Simplicity and compactness are additional features of the CVT.

The current research is the first article on CAD CVT. The scope of the current article is limited to (i) providing a conceptual understanding of the basic working mechanism of CAD CVT and (ii) providing a comprehensive analysis of important parameters of the CAD CVT. Therefore, the current research will focus on the design of CAD CVT, a detailed analysis of the transmission mechanism, a comprehensive analysis of (i) the transmission ratio (TR), (ii) the torque capacity, (iii) frictional losses, (iv) efficiency, and (v) pressure at traction points, and experimental verification of the basic functionality of CAD CVT.

2. Materials and Methods

2.1. Problem Statement

We aim to develop a CVT that can generate positive, negative, and neutral gear ratios without requiring an additional set of epicyclic gears and clutches. Moreover, the CVT should transmit torque through multiple traction points and can be designed for any amount of torque by increasing the number of traction points.

2.2. Design Conception

Design conception is an intuitive and iterative process. After following an iterative process of design, evaluation, and improvement, a novel design capable of solving the stated problem was accomplished. The new design consists of a set of circumferentially arranged disks (CADs), which have frictional contact with an input disk connected to an input shaft and an output disk connected to an output shaft. The 3D model, design configuration, and operating principle of the new CVT are given below.

2.2.1. 3D Model

To better visualize and communicate the design, a 3D model of the CVT has been developed. The new CVT can have any number of circumferentially arranged disks (CADs). However, the current paper focuses on a CVT with four CADs. The 3D Model of the new CVT has been developed and is shown in Figure 1a,b.

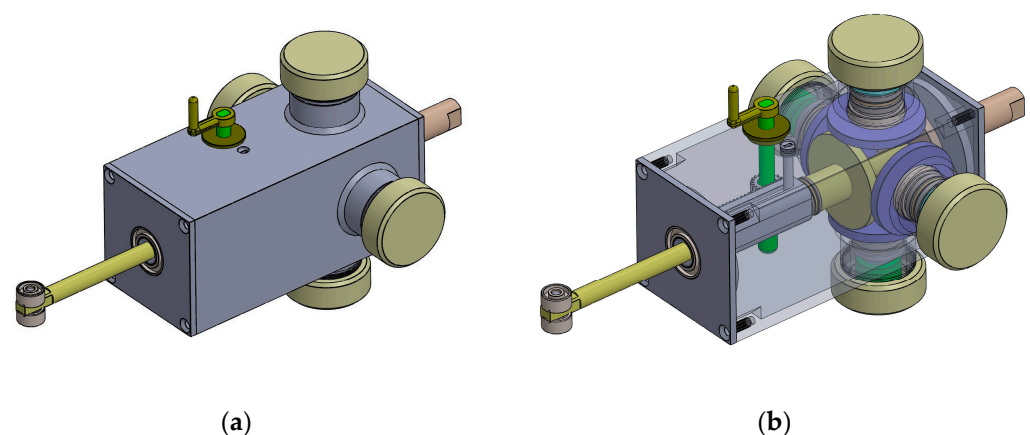


Figure 1. (a) CAD CVT with four CADs; (b) CAD CVT with two sides transparent for better viewing.

2.2.2. Configuration

To better understand the configuration of the proposed CVT, a 3D model with four traction points has been selected and numbered, as shown in Figures 2 and 3. A description of each numbered component is given in Table 1.

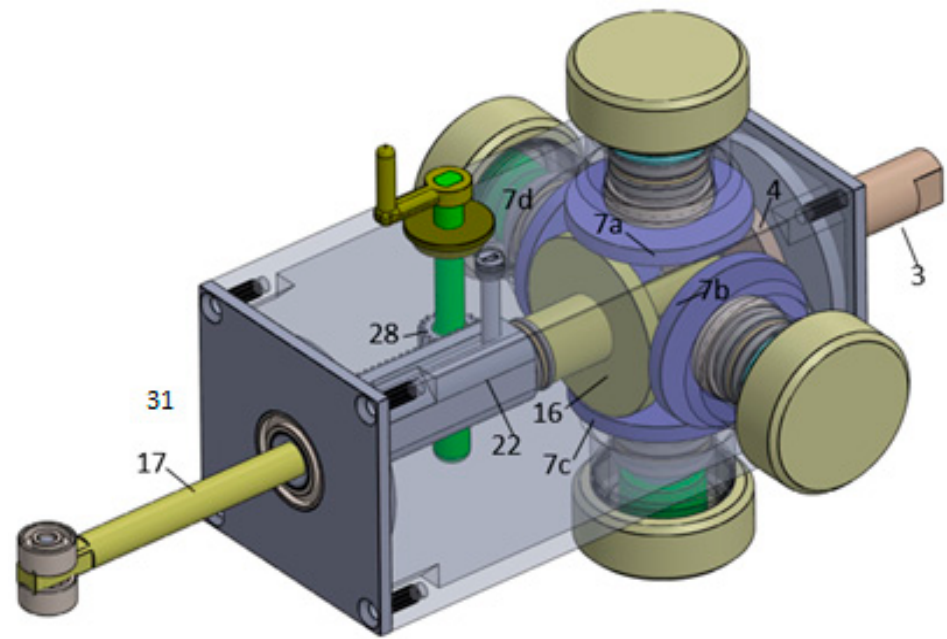


Figure 2. CAD CVT with four CADs.

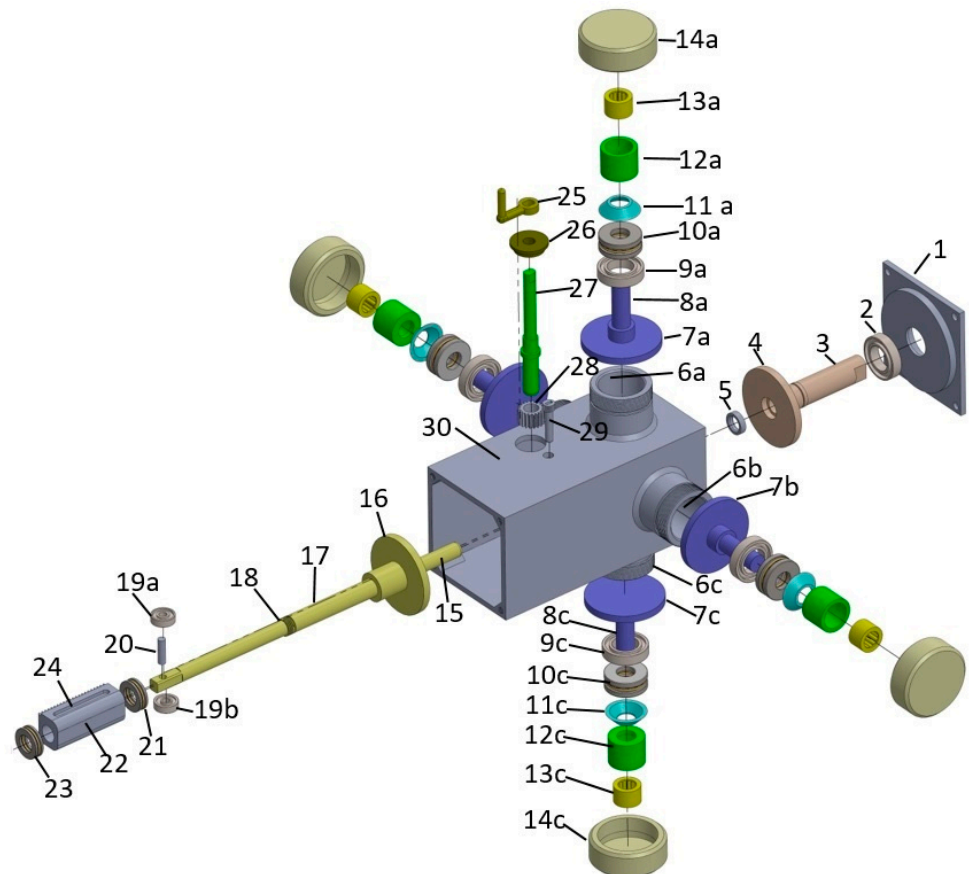


Figure 3. Exploded view of CAD CVT with four CADs.

Table 1. Description of part numbers shown in Figures 2 and 3.

| S.No | Part No | Description |
|------|-------------------------------|--|
| 1 | '1' | Input side lid. |
| 2 | '2' | Input shaft bearing. |
| 3 | '3' | Input Shaft |
| 4 | '4' | Input Disk |
| 5 | '5' | The alignment bearing fitted in input shaft '3' and alignment shaft '15' axially moves in it. |
| 6 | '6a', '6b', '6c', '6d' | Housing for accommodating circumferentially arranged disks '7a', '7b', '7c', '7d', and miscellaneous components. |
| 7 | '7a', '7b', '7c', '7d' | Circumferentially arranged disks. They have traction contact with input disk '4' and output disk '16'. The circumferentially arranged disks '7a', '7b', '7c', and '7d', along with input disk '4' and output disk '16', form the backbone of the proposed CVT design. |
| 8 | '8a', '8b', '8c', '8d' | Shafts of the circumferentially arranged disks '7a', '7b', '7c', '7d', respectively. |
| 9 | '9a', '9b', '9c', '9d' | Ball bearing for supporting one end of the shafts '8a', '8b', '8c', '8d', respectively. They keep the circumferentially arranged disks firmly in its place. Moreover it also helps in smooth rotary motion of the circumferentially arranged disks. |
| 10 | '10a', '10b', '10c', '10d' | Thrust bearing. They transfer the axial load provided by bellivele spring (Disk spring) to the circumferentially arranged disks without hindering the rotary motion of the circumferentially arranged disks. |
| 11 | '11a', '11b', '11c', '11d' | Bellivelle springs/Disk springs. They provide a continuous axial loading to the circumferentially arranged disks. It is because of the axial loading provided by these springs that traction between circumferentially arranged disks and input and output disk is produced. |
| 12 | '12a', '12b', '12c', '12d' | It is a sort of spacer which has two intended functions. Firstly it transfers axial load from Caps '14a', '14b', '14c' and '14d' to the respective disk springs. Secondly it acts as a housing for pin bearings '13a', '13b', '13c', and '13d'. |
| 13 | '13a', '13b', '13c', '13d' | Pin bearing which support the outer ends of shafts '8a', '8b', '8c' and '8d'. They help in keeping the circumferentially arranged disks in place and helps in their smooth rotation. |
| 14 | '14a', '14b', '14c', '14d' | Caps for CADs housing '6a', '6b', '6c', '6d'. It is also used for adjusting force applied on CADs. By tightening these caps we can increase the tractive force between CADs and input disk '4' and output disk '16'. |
| 15 | '15' | Alignment shaft. It is actually an extension of the output shaft. It can rotate and can also be moved axially inside the input shaft '3' via bearing '5'. It keeps the input shaft '4' and output shaft '17' perfectly aligned. |
| 16 | '16' | Output disk. It is connected to output shaft '17' and has a traction contact with circumferentially arranged disks. Its main purpose is to transfer motion from circumferentially arranged disks (CADs) to the output shaft. It is pertinent to mention that the location of its traction contact on the circumferentially arranged disks determines gear ratio. |
| 17 | '17' | Output shaft. |
| 18 | '18' | Threads on the output shaft for retaining axial movement of the rack '22'. |
| 19 | '19a', '19b' | These are roller bearings attached to the outermost end of the shaft. The load to be driven by CVT will have a shaft which will be square in shape from inside and must be hollow so that these roller bearing can be axially moved inside the hollow shaft. During changing gear ratio when the output shaft will be moved axially, these bearings will help in reduction of friction between the output shaft of the CVT and input shaft of the load. |
| 20 | '20' | Pin supporting bearing '19a' and '19b'. |
| 21 | '21' | Thrust bearing between rack '22' and output shaft '17'. This reduces friction between rack '22' and output shaft '17' when the output shaft is axially pushed towards the input shaft during gear ratio change. |
| 22 | '22' | Rack. It is part of the rack and pinion mechanism whose purpose is to move the output shaft in axial direction for gear ratio change. |
| 23 | '23' | Thrust bearing between rack '22' and output shaft '17'. This reduces friction between rack '22' and output shaft '17' when the output shaft is axially pushed away from the input shaft during gear ratio change. |
| 24 | '24' | Guiding slot in the rack '22'. This restricts the movement of the rack to axial direction only. |
| 25 | '25' | Handle for operating rack and pinion mechanism for gear ratio change. |
| 26 | '26' | Bus h/Bearing. |
| 27 | '27' | Pinion shaft. |
| 28 | '28' | A small spur gear acting as a pinion. |
| 29 | '29' | Guiding pin which sits in the guiding slot of the rack. |
| 30 | '30' | CVT casing. |
| 31 | '31' | Output Shaft Bearing. |

2.2.3. Operating Principle

The main operating principle of the current CVT is to vary the radius of traction points between the circumferentially arranged disks (CADs) and the output disk. This is achieved by axial movement of the output disk through a rack-and-pinion arrangement. Detailed functionality is elaborated below. Moreover, for a better understanding, refer to Figures 2 and 3.

When clockwise rotation is applied to input shaft '3', it results in clockwise rotation of input disk '4'. This results in the anti-clockwise rotation of circumferentially arranged disks '7a', '7b', '7c', and '7d', which are in traction contact with input disk '4'. Since output disk '16' is in traction contact with the circumferentially arranged disks (CADs), depending on the position of the output disk, it may result in anti-clockwise, clockwise, or no motion when seen from the input side. Moreover, the speed of rotation of the output is also influenced by the radius of contact between the output disk and CADs. This is illustrated in Figures 4 and 5.

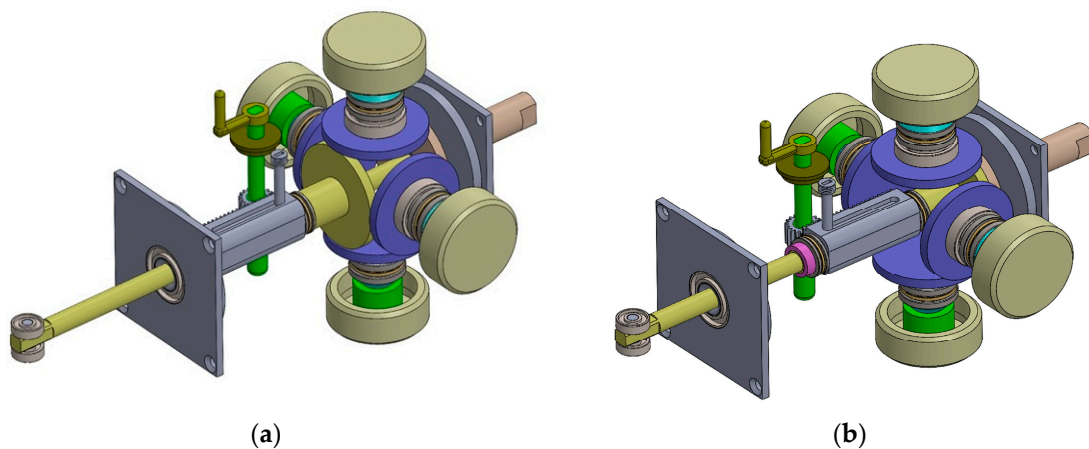


Figure 4. (a) CAD CVT in Normal mode; (b) CAD CVT in reverse mode.

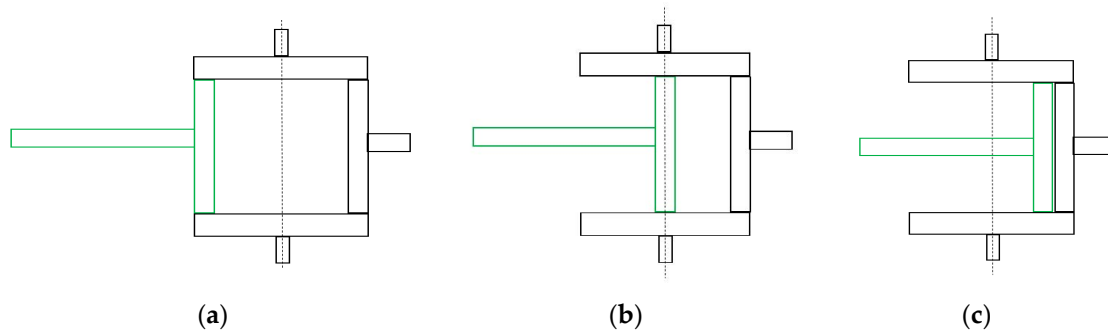


Figure 5. (a) Normal Mode. (b) Neutral Mode. (c) Reverse Mode.

In order to maintain the traction contact, circumferentially arranged disks '7a', '7b', '7c', and '7d' are continuously pressed by disk springs '11a', '11b', '11c', and '11d' in the axial direction. Moreover, thrust bearings '10a', '10b', '10c', and '10d' ensure smooth movement of the circumferentially arranged disks in the presence of axial loading due to the disk spring.

Different gear ratios including positive, negative, and zero are achieved through axial movement of output disk '16' through the rack-and-pinion mechanism ('22' and '28'). This mechanism is designed such that it does not hinder the rotary motion of the output shaft. This is achieved by making a throughout hole in the rack through which the output shaft can move freely. Moreover, a set of thrust bearings ('21' and '23') on each end of the rack ensures that no sliding friction is generated between the rack and the output shaft,

especially during gear ratio change. An important feature of the gear-changing mechanism is that guiding slot '24' has been introduced in the rack. This ensures that the rack will not experience any rotary motion and the motion of the rack is restricted to predefined limits in the axial direction.

An important feature of the current CVT is the utilization of two bearings at the end of the output shaft. The input shaft of the load to which the output shaft of the CVT will be attached will consist of a square hole in which the two bearings will be able to move. The bearing will enable smooth axial movement of the output shaft of the CVT in the input shaft of the load.

2.3. Transmission Ratio

In order to calculate the transmission ratio, consider Figure 6.

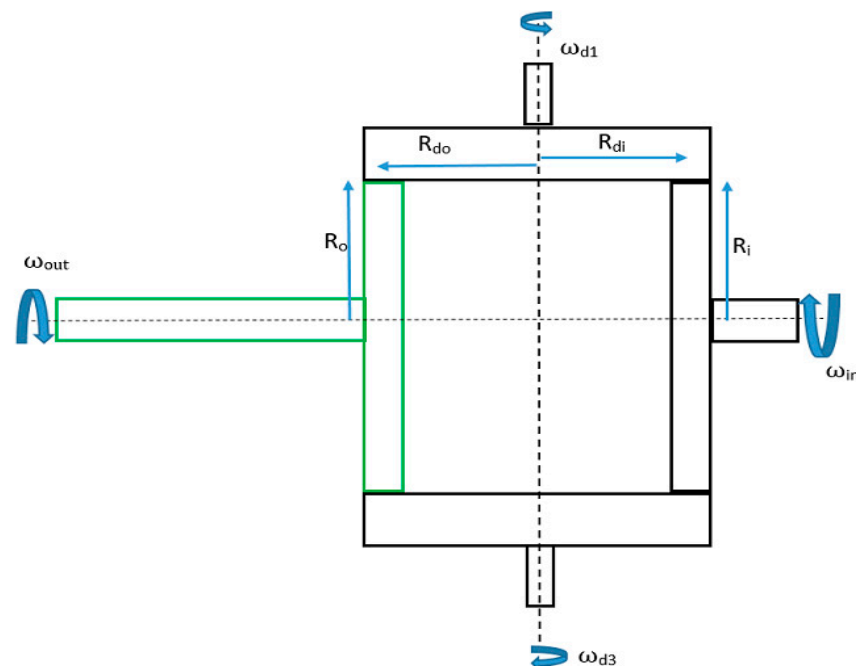


Figure 6. 2D side view of CAD CVT with four circumferentially arranged disks (CADs).

Let

R_{di1} = Distance between Circumferentially Arranged Disk (CAD) no 1 and the traction point of CAD 1 with the input disk.

R_{di2} = Distance between Circumferentially Arranged Disk (CAD) no 2 and the traction point of CAD 2 with the input disk.

R_{din} = Distance between Circumferentially Arranged Disk (CAD) no n and the traction point of CAD n with the input disk.

R_{do1} = Distance between Circumferentially Arranged Disk (CAD) no 1 and the traction point of CAD 1 with the output disk.

R_{do2} = Distance between Circumferentially Arranged Disk (CAD) no 2 and the traction point of CAD 2 with the output disk.

R_{don} = Distance between Circumferentially Arranged Disk (CAD) no n and the traction point of CAD n with the output disk.

ω_{d1} = speed of CAD 1.

ω_{d2} = speed of CAD 2

ω_{dn} = speed of CAD n.

ω_{in} = speed of input disk/input shaft.

ω_{out} = speed of output disk/output shaft.

We assume that all CADs have the same shape and size and that their axes of rotation lie in the same plane. Furthermore, the output disk and the input disk have the same shape and size and their axes of rotation are perpendicular to the plane containing the axis of rotation of CADs. Then we can write

$$\mathbf{R}_{di1} = \mathbf{R}_{di2} = \mathbf{R}_{din} = \mathbf{R}_{di} \quad (1)$$

$$\mathbf{R}_{do1} = \mathbf{R}_{do2} = \mathbf{R}_{don} = \mathbf{R}_{do} \quad (2)$$

$$\omega_{d1} = \omega_{d2} = \omega_{dn} = \omega_d \quad (3)$$

It is pertinent to mention that if the axes of rotation of CADs do not lie in the same plane, then each CAD will rotate at different speeds. In this situation, each CAD will try to rotate the output disk at different speeds. This will result in slippage at the traction points of CADs.

Having established the conditions for proper operation of the CAD CVT, we can calculate the transmission ratio as follows:

$$\text{TR} = \frac{\omega_o}{\omega_i} \quad (4)$$

From Figure 6, we can write

$$\frac{\omega_d}{\omega_i} = \frac{R_i}{R_{di}} \quad (5)$$

$$\omega_d = \frac{R_i}{R_{di}} \omega_i \quad (6)$$

$$\frac{\omega_d}{\omega_o} = \frac{R_o}{R_{do}} \quad (7)$$

$$\omega_d = \frac{R_o}{R_{do}} \omega_o \quad (8)$$

$$\frac{R_i}{R_{di}} \omega_i = \frac{R_o}{R_{do}} \omega_o \quad (9)$$

From Figure 6, we can write

$$R_i = R_o \quad (10)$$

The Transmission Ratio can be defined as

$$\text{TR} = \frac{\omega_o}{\omega_i} \quad (11)$$

$$\frac{\omega_o}{\omega_i} = \frac{R_{do}}{R_{di}} \quad (12)$$

So

$$\text{TR} = \frac{R_{do}}{R_{di}} \quad (13)$$

Now, from Figure 6, R_{do} can be positive, zero, or negative; therefore, for an accurate prediction of the transmission ratio, we should consider R_{do} as a vector quantity. So, we can write Equation (13) as

$$\text{TR} = \frac{\vec{R}_{do}}{R_i} \quad (14)$$

If t is the thickness of the input disk and the output disk, then $R_{do} = [R_{di} - R_{di} + t]$. The transmission ratio is shown in the graph in Figure 7.

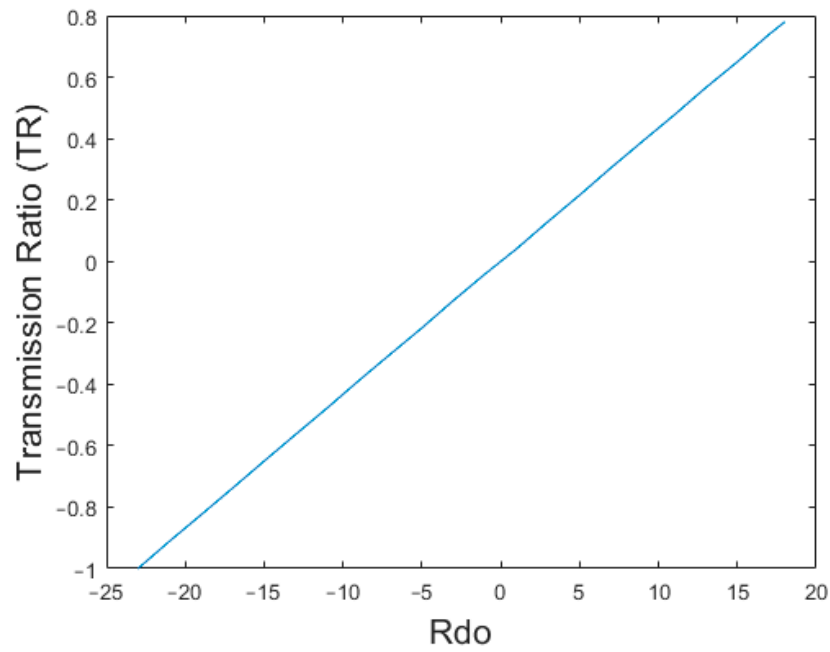


Figure 7. Graph showing transmission ratio vs. R_{do} .

2.4. Torque Capacity

In order to calculate the maximum torque capacity of the new CVT, we consider Figure 8. For the sake of simplicity, we confine our scope to a case in which the Transmission Ratio $TR = -1$.

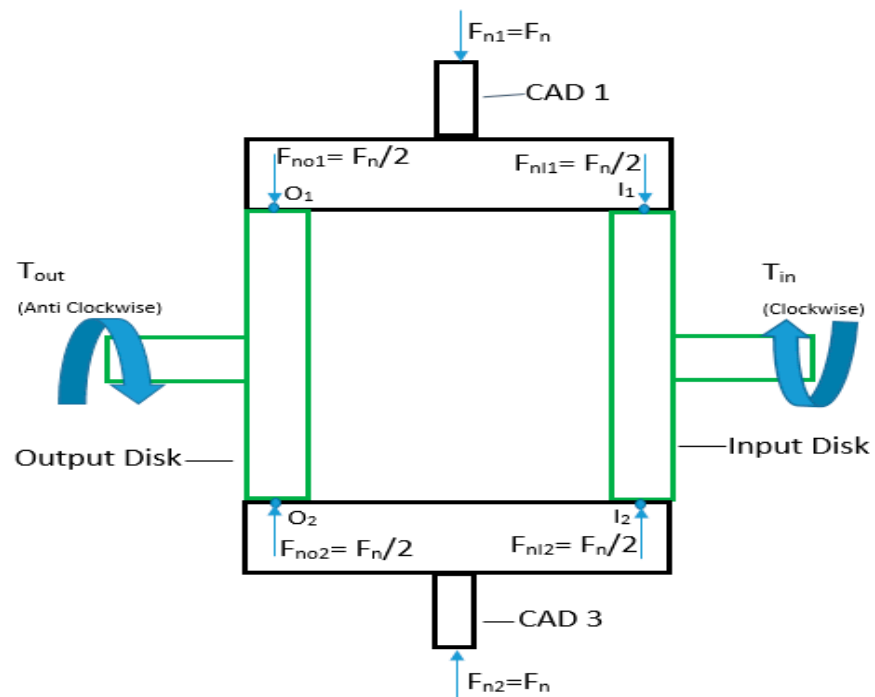


Figure 8. Two-dimensional side view of CAD CVT with four circumferentially arranged disks, depicting tractive forces between the circumferentially arranged disks and input disk and output disk.

F_n is the force applied to the CAD along its axis of rotation and normal to the tractive surface of the CAD. Then, the force applied by the CAD to the input disk and output disk at their respective traction points is

$$F_{no} = \frac{1}{2}F_n \quad (15)$$

$$F_{ni} = \frac{1}{2}F_n \quad (16)$$

The traction force generated at point $O1$ is F_{TO1} where

$$F_{TO1} = F_{no1}\mu_{kt}\mu_{kt} \quad (17)$$

$$F_{TO1} = \frac{1}{2}F_n\mu_{kt} \quad (18)$$

where μ_{kt} is the coefficient of kinematic traction.

Similarly,

$$F_{TI1} = F_{ni1}\mu_{kt} \quad (19)$$

$$F_{TI1} = \frac{1}{2}F_n\mu_{kt} \quad (20)$$

Now, the torque generated at the output shaft due to traction at point $O1$ is

$$T_{cO1} = F_{TO1}R_o \quad (21)$$

$$T_{cO1} = \frac{1}{2}F_n\mu_{kt}R_o \quad (22)$$

Now, if there are n circumferentially arranged disks in the CVT, then the total torque capacity of the CVT can be calculated as follows:

$$T_c = T_{cO1} + T_{cO2} + T_{cO3} + \dots + T_{cOn} \quad (23)$$

$$T_c = (F_{TO1}R_o + F_{TO2}R_o + F_{TO3}R_o + \dots + F_{TOn}R_o) \quad (24)$$

$$T_c = R_o(F_{TO1} + F_{TO2} + F_{TO3} + \dots + F_{TOn}) \quad (25)$$

$$T_c = R_o \sum_{i=1}^n F_{TOi} \quad (26)$$

$$T_c = R_o \sum_{i=1}^n \frac{1}{2}F_n\mu_{kt} \quad (27)$$

$$T_c = nR_o \frac{1}{2}F_n\mu_{kt} \quad (28)$$

In the above equation:

n = number of circumferentially arranged disks.

R_o = Radius of output disk.

F_n = Load applied to CADs.

μ_{kt} = Coefficient of Kinematic traction of the material of which CAD and output disk is made.

Figure 9 shows a graph of torque capacities of different CAD CVTs with $n = 4$, $n = 10$, and $n = 20$.

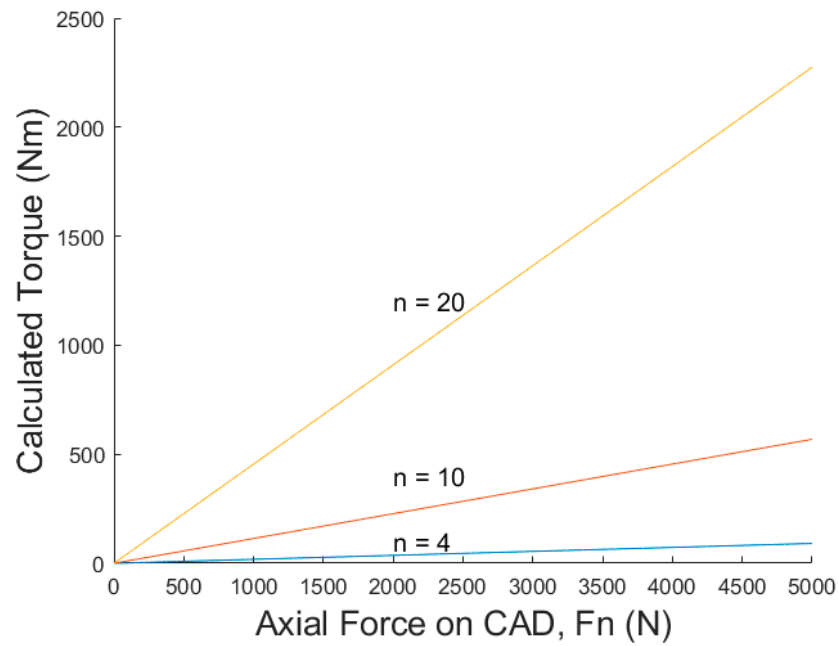


Figure 9. Torque capacity of CAD CVT for different numbers of CADs. Transmission Ratio, $TR = -1$. $\mu_{kt} = 0.35$, $R_o = 26$ mm for $n = 4$, $R_o = 2.5 \times 26$ mm for $n = 10$, $R_o = 5 \times 26$ mm for $n = 20$.

2.5. Frictional Losses and Efficiency

2.5.1. Spin Losses

To calculate spin losses, we consider Figure 10.

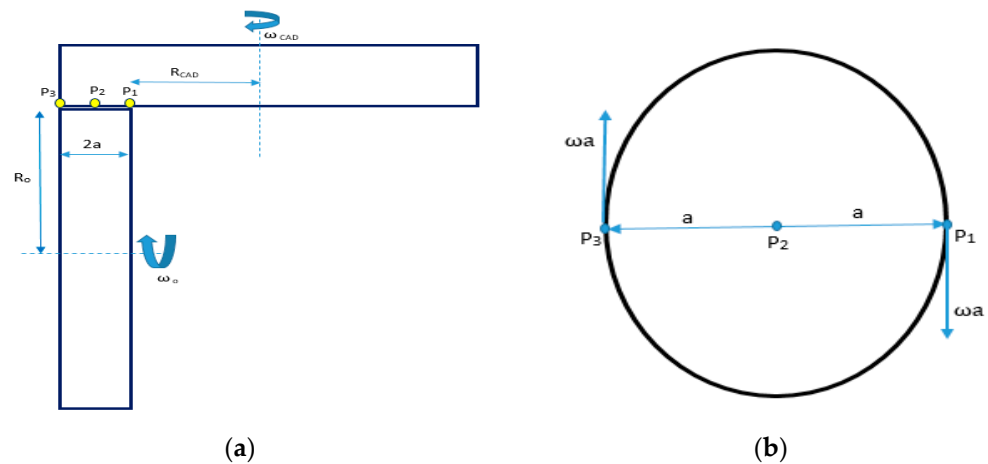


Figure 10. (a) CAD in frictional contact with output disk. (b) Spinning of different points of CAD, which are in frictional contact with output disk.

In Figure 10a, a CAD is in frictional contact with an output disk. Let P1, P2, and P3 be three points on the portion of the CAD, which is in frictional contact with the rim of the output disk. These three points lie on a line that is perpendicular to the axis of rotation of the CAD and parallel to the axis of rotation of the output disk. P1 represents the innermost point of the contact portion and P3 represents the outermost point of the contact portion. P2 is halfway between P1 and P3.

When the CAD rotates, P1, P2, and P3 have different linear velocities because they have different distances from the axis of rotation of CAD. These three points try to pull the corresponding points on the output disk with the same velocity with which they themselves are moving. However, the corresponding points on the output disk have the same distance

from the axis of rotation of the output disk; therefore, they must have the same linear velocity. This results in a phenomenon where the set of points lying between P1 and P3 on the contact portion of the CAD experience a spinning effect as shown in Figure 10b. The frictional losses due to the spinning effect are calculated as follows:

Let

$$\begin{aligned}\omega_{CAD} &= \text{Spinning speed of CAD} \\ &= \omega\end{aligned}$$

Then, from Figure 10 we can write

$$V_{p1} = R_{CAD}\omega \quad (29)$$

$$V_{p2} = (R_{CAD} + a)\omega \quad (30)$$

$$V_{p3} = (R_{CAD} + 2a)\omega \quad (31)$$

$$V_{p2} - V_{p1} = \omega a \quad (32)$$

$$V_{p3} - V_{p2} = \omega a \quad (33)$$

Now, let

$$V_{p2} = 0 \quad (34)$$

Then, from Equations (32) and (33) we can write

$$V_{p1} = -\omega a \quad (35)$$

And

$$V_{p3} = \omega a \quad (36)$$

Then, from Figure 10, we can write

$$\omega_{CAD} = \omega \quad (37)$$

$$V_s = \omega a \quad (38)$$

$$P_s = \tau_s \omega \quad (39)$$

$$\tau_s = \tau_{s1} + \tau_{s2} \quad (40)$$

$$\tau_{s1} = \int_0^a F \cdot x dx \quad (41)$$

$$\tau_{s1} = \int_0^a \frac{F_n \mu_s}{2a} \cdot x dx \quad (42)$$

$$\tau_{s1} = \frac{F_n \mu_s}{2a} \frac{a^2}{2} \quad (43)$$

$$\tau_{s1} = \frac{F_n \mu_s a}{4} \quad (44)$$

$$\tau_{s2} = \int_{-a}^0 F \cdot x dx \quad (45)$$

$$\tau_{s2} = \int_{-a}^0 \frac{-F_n \mu_s}{2a} \cdot x dx \quad (46)$$

$$\tau_{s2} = \frac{-F_n \mu_s}{2a} \frac{-a^2}{2} \quad (47)$$

$$\tau_{s2} = \frac{F_n \mu_s a}{4} \quad (48)$$

From Equation (40)

$$\tau_s = \frac{1}{2} F_n \mu_s a \quad (49)$$

And from Equation (39)

$$P_s = \frac{1}{2} F_n \mu_s a \omega \quad (50)$$

Equation (50) shows the power loss due to spinning at a single traction point.

2.5.2. Rolling Friction Losses

In addition to spin losses, rolling friction is also generated between the circumferentially arranged disks (CADs) and the input and output disks. The power losses generated by rolling friction are as follows:

Let μ_r = coefficient of rolling friction.

Then, the resistive forces generated by the normal force F_n at the traction point of the input disk and the output disk are

$$F_{ri} = \frac{1}{2} F_n \mu_r \quad (51)$$

$$F_{ro} = \frac{1}{2} F_n \mu_r \quad (52)$$

And the resistive torque generated is

$$T_{ri} = \frac{1}{2} F_n \mu_r R_i \quad (53)$$

$$T_{ro} = \frac{1}{2} F_n \mu_r R_o \quad (54)$$

And the corresponding power loss is

$$P_{Fri} = \frac{1}{2} F_n \mu_r R_i \omega_i \quad (55)$$

$$P_{Fro} = \frac{1}{2} F_n \mu_r R_o \omega_o \quad (56)$$

As

$$R_i = R_o = R \quad (57)$$

And

$$\omega_i = \omega_{CAD} \frac{R_{di}}{R_i} \quad (58)$$

And

From Equation (11), for the transmission ratio, $TR = -1$ or $TR = 1$, $|\omega_o| = |\omega_i|$, so we can write Equations (55) and (56) as follows:

$$P_{Fri} = \frac{1}{2} F_n \mu_r R_i \omega_{CAD} \frac{R_{di}}{R_i} \quad (59)$$

$$P_{Fro} = \frac{1}{2} F_n \mu_r R_i \omega_{CAD} \frac{R_{di}}{R_i} \quad (60)$$

Equations (59) and (60) can be further simplified as

$$P_{Fri} = \frac{1}{2} F_n \mu_r \omega_{CAD} R_{di} \quad (61)$$

$$P_{Fro} = \frac{1}{2} F_n \mu_r \omega_{CAD} R_{di} \tag{62}$$

2.5.3. Bearing Losses

After spin losses, the major frictional losses are in the bearings supporting the circumferentially arranged disks (CADs). The bearing losses are calculated as follows:

Let:

T_o = torque at the output shaft.

T_{omax} = maximum torque that can be supported by the output shaft.

T_{in} = torque at the input shaft.

From Figure 11, it can be observed that when the transmission ratio, $TR = -1$, then

$$T_{omax} + T_{in} = \text{maximum} \tag{63}$$

Equation (63) defines a condition in which the bearings of the CAD experience maximum load and hence maximum bearing losses.

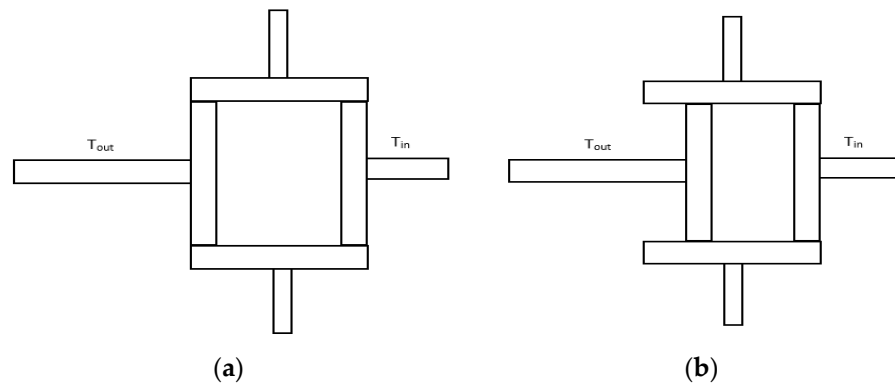


Figure 11. (a) CAD CVT with Transmission ratio, $TR = -1$ (b) $-1 < TR < 0$.

We assume that the output shaft of the CVT is subjected to the maximum torque that it can support and $TR = -1$. In this condition, the free-body diagram of a single CAD is given in Figure 12.

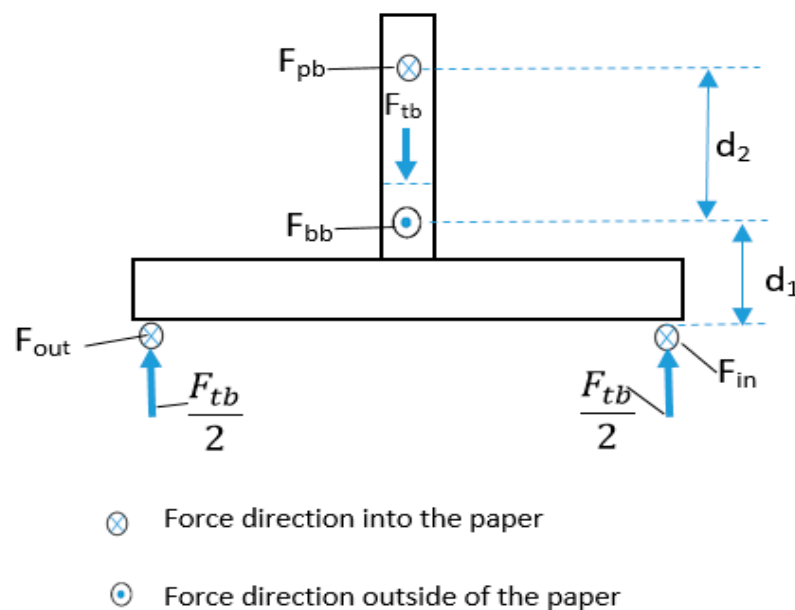


Figure 12. Free-body diagram of a CAD when $TR = -1$.

Let

F_{out} = Force applied by output disk on CAD at the traction point.

F_{in} = Force applied by input disk on CAD at traction point.

F_{bb} = Force applied by ball bearing on CAD.

F_{pb} = Force applied by pin bearing on CAD.

F_{tb} = Force applied by thrust bearing on CAD.

R_{bb} = Radius of ball bearing.

R_{pb} = Radius of pin Bearing.

R_{tb} = Radius of thrust bearing.

Then

From the free-body diagram, we can write

$$F_{bb} = F_{out} + F_{in} + F_{pb} \quad (64)$$

For $TR = -1$, we can write

$$F_{out} = F_{in} = F \quad (65)$$

So, Equation (64) becomes

$$F_{bb} = 2F + F_{pb} \quad (66)$$

And

$$F_{pb}d_2 = 2Fd_1 \quad (67)$$

$$F_{pb} = 2F \frac{d_1}{d_2} \quad (68)$$

From Equations (66) and (68),

$$F_{bb} = 2F + 2F \frac{d_1}{d_2} \quad (69)$$

From Equations (18) and (20), we can write

$$F = \frac{1}{2}F_n\mu_{kt} \quad (70)$$

So, Equations (68) and (69) become

$$F_{pb} = F_n\mu_{kt} \frac{d_1}{d_2} \quad (71)$$

$$F_{bb} = F_n\mu_{kt} + F_n\mu_{kt} \frac{d_1}{d_2} \quad (72)$$

The force applied by thrust bearing F_{tb} is equal to F_n . Therefore,

$$F_{tb} = F_n \quad (73)$$

The coefficient of friction of a bearing is not constant and depends on a number of factors including tribological factors. However, the variation is normally very small; therefore, for the sake of simplicity, we assume it to be constant.

We can calculate the power loss in the bearings as follows:

$$P_{bb} = \mu_{bb}F_{bb}R_{bb}\omega_{CAD} \quad (74)$$

$$P_{bb} = \mu_{bb}(F_n\mu_{kt} + F_n\mu_{kt} \frac{d_1}{d_2})R_{bb}\omega_{CAD} \quad (75)$$

$$P_{pb} = \mu_{pb}F_{pb}R_{pb}\omega_{CAD} \quad (76)$$

$$P_{pb} = \mu_{pb} F_n \mu_{kt} \frac{d_1}{d_2} R_{pb} \omega_{CAD} \quad (77)$$

$$P_{tb} = \mu_{bb} F_{tb} R_{tb} \omega_{CAD} \quad (78)$$

$$P_{tb} = \mu_{bb} F_n R_{tb} \omega_{CAD} \quad (79)$$

2.5.4. Total Frictional Losses

Assuming that spin losses at traction points, friction losses due to rolling friction at traction points, and frictional losses in bearings supporting the circumferentially arranged disks are major frictional losses in the CVT, we can write the total frictional losses of the CVT as follows:

$$P_{Total} = n \{ (P_{sI} + P_{so}) + (P_{Fri} + P_{Fro}) + (P_{bb} + P_{pb} + P_{tb}) \} \quad (80)$$

In Equation (80),

P_{Total} = Total power losses due to friction.

P_{sI} = Power loss due to spin at tractive contact of input disk and CAD.

P_{so} = Power loss due to spin at tractive contact of output disk and CAD.

P_{Fri} = Power loss due to rolling friction at tractive contact of input disk and CAD.

P_{Fro} = Power loss due to rolling friction at tractive contact of input disk and CAD.

P_{bb} = Power loss in ball bearing supporting CAD.

P_{pb} = Power loss in pin bearing supporting CAD.

P_{tb} = Power loss in thrust bearing supporting CAD.

n = Number of CAD in the CVT.

Since maximum bearing losses occur when $TR = -1$, we calculate total frictional losses at $TR = -1$ as follows:

$$P_{Total} = n \left[\left(\frac{1}{2} F_n \mu_s a \omega_{CAD} + \frac{1}{2} F_n \mu_s a \omega_{CAD} \right) + \left(\frac{1}{2} F_n \mu_r \omega_{CAD} R_{di} + \frac{1}{2} F_n \mu_r \omega_{CAD} R_{di} \right) + \left(\mu_{bb} (F_n \mu_{kt} + F_n \mu_{kt} \frac{d_1}{d_2}) R_{bb} \omega_{CAD} + (\mu_{pb} F_n \mu_{kt} \frac{d_1}{d_2} R_{pb} \omega_{CAD}) + (\mu_{tb} F_n R_{tb} \omega_{CAD}) \right) \right] \quad (81)$$

$$P_{Total} = n F_n \omega_{CAD} \left[(\mu_s a) + (\mu_r R_{di}) + \left(\mu_{bb} \mu_{kt} R_{bb} \left(1 + \frac{d_1}{d_2} \right) + \left(\mu_{pb} \mu_{kt} R_{pb} \frac{d_1}{d_2} \right) + (\mu_{tb} R_{tb}) \right) \right] \quad (82)$$

Power loss at different rotation speeds (ω), forces applied on CADs (F_n), and lengths of contact area ($2a$) are plotted in Figures 13–15. Power loss is expressed in Watt, force applied to CADs is expressed in Newton, and the rotation speed of CADs is expressed in rad/sec. The force is varied from 0 to 5 kN and the rotation speed of CADs (ω) is 50, 100, 150, 200, and 250 rad/sec. The length of the contact area is equal to $2a$. Power losses at $a = 2.5$ mm, $a = 1$ mm, and $a = 0.5$ mm are calculated. For all graphs shown in Figures 13–15, the constant parameters are the number of CADs, $n = 4$, $\mu_s = 0.42$, $\mu_r = 0.002$, $a = 0.0025$ m, $R_{di} = 0.025$ m, $\mu_{bb} = 0.001$, $\mu_{tb} = 0.001$, $\mu_{pb} = 0.002$, $\mu_{kt} = 0.35$, $d_1 = 0.0085$ m, $d_2 = 0.0275$ m, $R_{bb} = 0.0085$ m, $R_{pb} = 0.005$ m, and $R_{tb} = 0.006$ m.

2.5.5. Efficiency

$$\text{Efficiency, } E = \frac{\text{Output power, } P_o}{\text{Input Power, } P_{in}} \quad (83)$$

$$P_{in} = P_o + \text{Total Frictional Losses } (P_{Total}) \quad (84)$$

$$E = \frac{P_o}{P_o + P_{Total}} \quad (85)$$

$$P_o = \tau_o \omega_o \quad (86)$$

τ_o represents torque at the output shaft and can be calculated using Equation (28). P_{Total} represents the total frictional losses and can be calculated using Equation (82)

The efficiency of CAD CVT has been calculated using Equations (28), (82), (85) and (86) and is given in Table 2. Moreover, the values of the constants assumed in these Equations are $n = 4$, $F_n = 5$ KN, Transmission Ratio, $TR = -1$. $\mu_{kt} = 0.35$, $R_o = 26$ mm, $\mu_s = 0.42$, $\mu_r = 0.002$, $a = 0.0025$ m, $R_{di} = 0.025$ m, $\mu_{bb} = 0.001$, $\mu_{tb} = 0.001$, $\mu_{pb} = 0.002$, $d_1 = 0.0085$ m, $d_2 = 0.0275$ m, $R_{bb} = 0.0085$ m, $R_{pb} = 0.005$ m, and $R_{tb} = 0.006$ m.

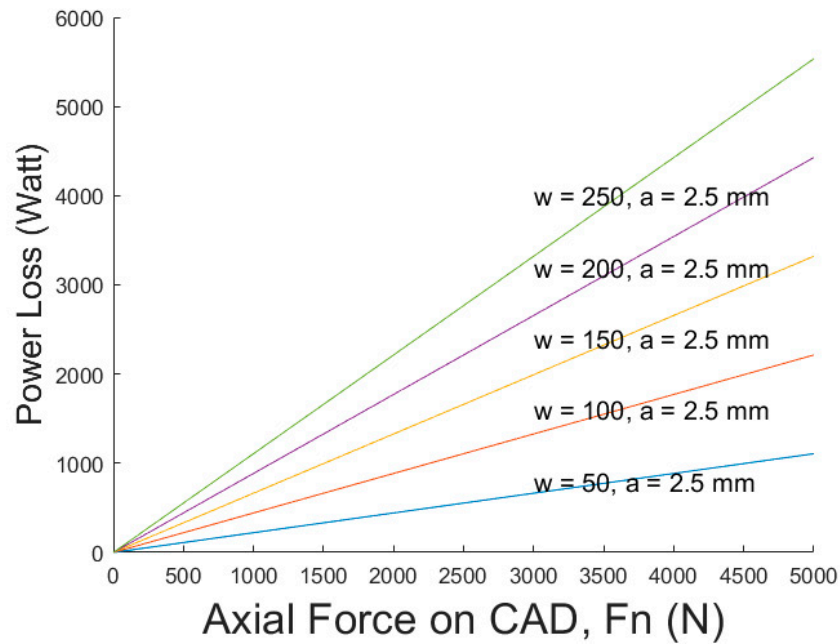


Figure 13. Power Loss due to friction of a CAD CVT with $n = 4$, $a = 2.5$ mm, and $\omega = \{50,100,150,200,250\}$.

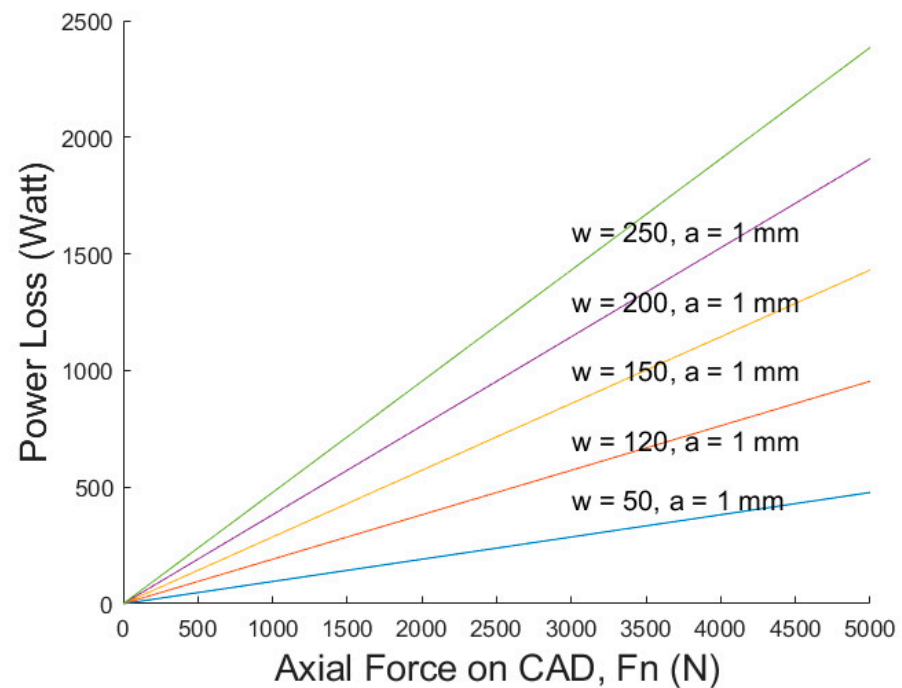


Figure 14. Power Loss due to friction of a CAD CVT with $n = 4$, $a = 1$ mm, and $\omega = \{50,100,150,200,250\}$.

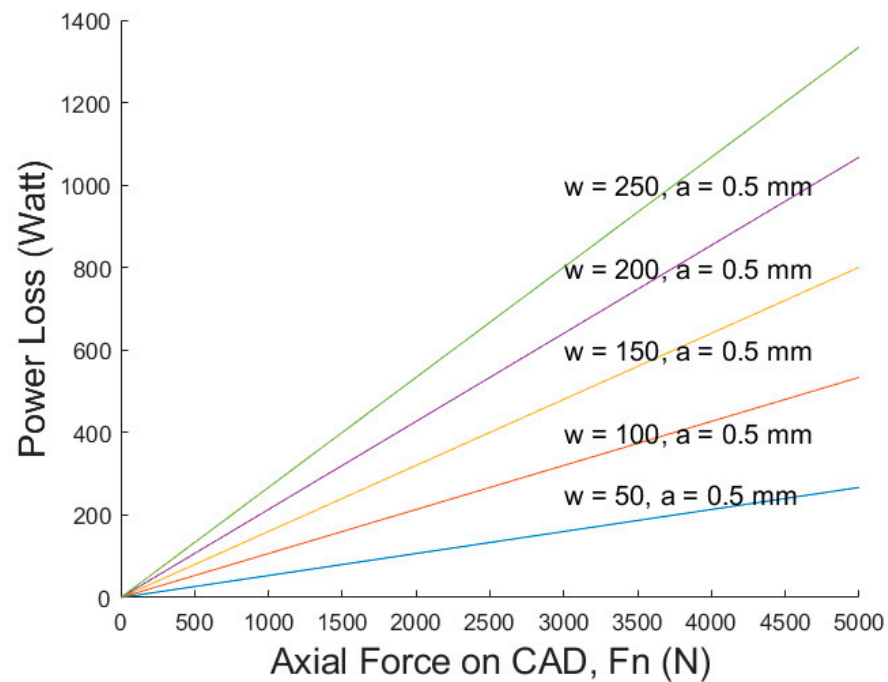


Figure 15. Power Loss due to friction of a CAD CVT with $n = 4$, $a = 0.5$ mm, and $\omega = \{50,100,150,200,250\}$.

Table 2. Maximum efficiency at different contact lengths.

| S. No | Contact Length 2a (mm) | No of CADs n | Rotation Speed ω_o (rad/sec) | Efficiency |
|-------|---------------------------|-----------------|--|------------|
| 1 | 2×2.5 mm | 4 | 250 | 79% |
| 2 | 2×1 mm | 4 | 250 | 90.56% |
| 3 | 2×0.5 mm | 4 | 250 | 94.4% |

2.6. Contact Pressure

It is important to calculate the maximum contact pressure at the traction points of CADs in order to ensure that the stress at the traction points does not exceed the limit of 2.5 GPa, which can be supported by commercially available steel grades.

In order to calculate the maximum pressure at the traction point, we will use the Hertz contact Stress Model for a Cylinder in Contact with a Plane [31]. In this model, the maximum pressure at a contact point is given by the following formula:

$$P_{\max} = \frac{2F}{\pi bL} \quad (87)$$

where:

F = Force applied.

L = length of Cylinder.

If both the cylinder and Plane are made of the same material, then we can write

$$b = \sqrt{\left(\frac{2F}{\pi L} \frac{\left(\frac{2(1-\nu^2)}{E} \right)}{\frac{1}{d}} \right)} \quad (88)$$

where:

E = Elastic moduli of the Material (210 GPa for steel).

ν = Poisson Ratio (0.3 for steel).

L = Length of cylinder.

d = diameter of the cylinder (0.052 m for the CAD CVT designed in this article.)

The maximum contact pressure of CAD CVT with $n = 4$, $n = 10$, and $n = 20$ was calculated using Equations (87) and (88). For each CVT, contact stress was calculated for $a = 0.5$ mm, $a = 1$ mm, and $a = 2.5$ mm corresponding to contact lengths of $L = 1$ mm, $L = 2$ mm, and $L = 5$ mm, respectively. The material for both the cylinder and the plane is steel, with $E = 210$ GPa and a Poisson ratio of $\nu = 0.3$. The graphs of calculations are shown in Figures 16–18.

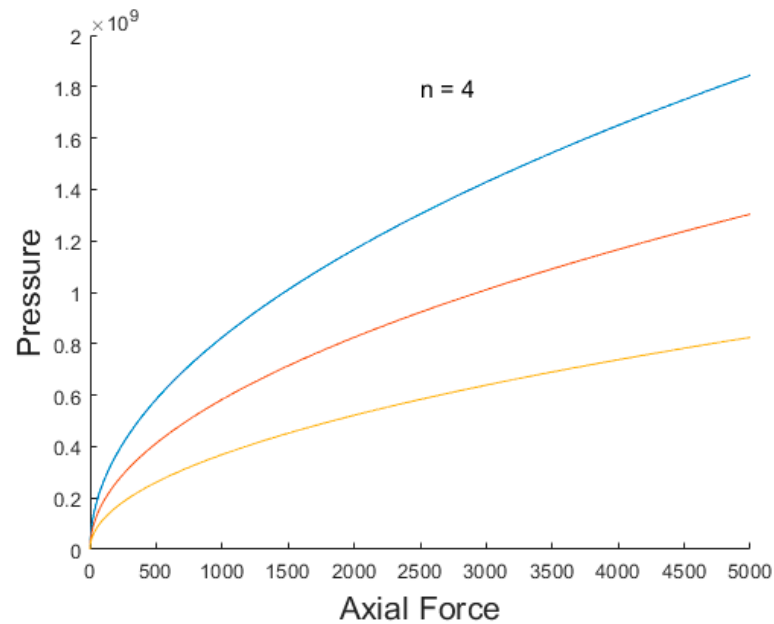


Figure 16. Pressure (Pascal) vs. Axial Force F_n (N) for CAD CVT with $n = 4$ and contact lengths of $L = 1$ mm (blue), $L = 2$ mm (red), and $L = 5$ mm (yellow).

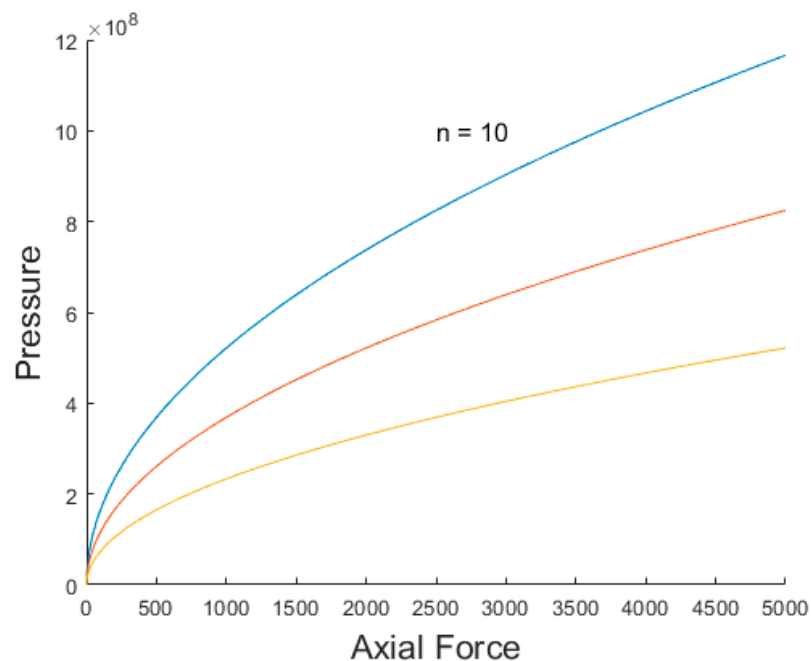


Figure 17. Pressure (Pascal) vs. Axial Force F_n (N) for CAD CVT with $n = 10$ and contact lengths of $L = 1$ mm (blue), $L = 2$ mm (red), and $L = 5$ mm (yellow).

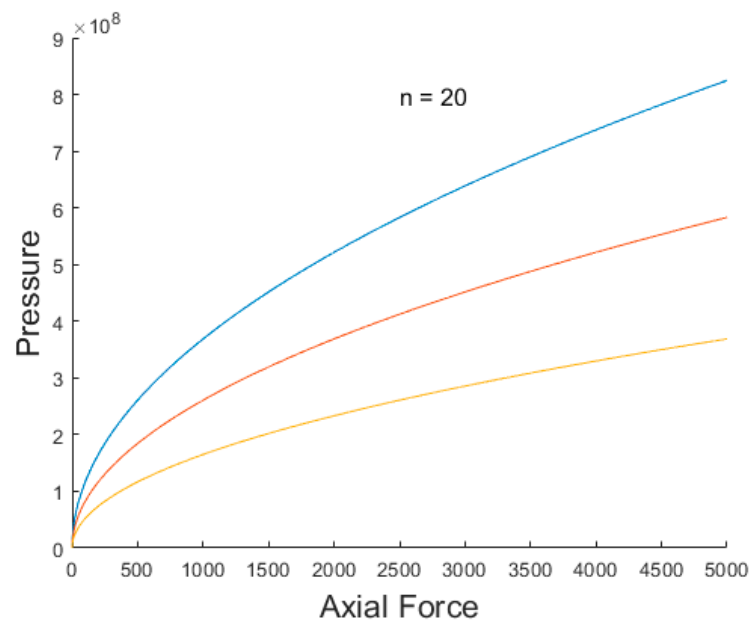


Figure 18. Pressure (Pascal) vs. Axial Force F_n (N) for CAD CVT with $n = 20$ and contact lengths of $L = 1$ mm (blue), $L = 2$ mm (red), and $L = 5$ mm (yellow).

2.7. Experimental Validation/Proof of Concept

In order to verify the proposed design, a Proof of Concept (PoC) was manufactured. The PoC was manufactured as per the model given in Figures 1–3. The main purpose of the PoC was to verify the basic functionality of the CAD CVT, which is:

- a. The CAD CVT should provide a continuum of gear ratios between two points.
- b. The CAD CVT should be able to provide positive, negative, and neutral gear ratios without the requirement of an additional gear set.

An experimental setup was established. The following procedure was adopted for the experiment:

- Step 1: Displace the output shaft fully outward through the gear ratio changing lever.
- Step 2: Measure the length of the output shaft.
- Step 3: Rotate the input shaft by 360° (2π).
- Step 4: Measure the corresponding rotation of the output shaft.
- Step 5: Displace the output shaft inward by 2 mm.
- Step 6: If the output shaft cannot be displaced further, then move to step 7; otherwise, return to step 2.
- Step 7: End.

The data recorded during the experiment are shown in Table 3. The corresponding graphs are shown in Figures 19 and 20. Experimental setup of the experiment is shown in Figure 21a.

Figure 21b represents the CAD CVT in its fully assembled form. The thin long shaft observable in Figure 21b is the output shaft. In Figure 21c, the lid from the output shaft side is removed and we can see the inside of the CAD CVT from the output shaft side. The rack-and-pinion mechanism can be clearly seen. In Figure 21d, the output shaft along with the rack-and-pinion mechanism has been removed. As a result, the four CADs and the input disk can be seen. Figure 21e,f shows the CAD CVT from the input shaft side. Figure 21g shows the four CADs from the input side. Figure 21h shows all components of the CAD CVT. Each CAD is supported by a ball bearing, a thrust bearing, and a pin bearing. Moreover, a disk spring continuously presses the CAD through the thrust bearing so that the CAD can maintain frictional contact with the input and output disks, and thus, smooth operation of the mechanism is possible. The thrust bearing eliminates the friction between the disk spring and the CAD. Two thrust bearings at each end of the rack can also

be observed. They help eliminate sliding friction between the output shaft and the rack during gear-changing operations. The Proof of Concept has demonstrated that different parts of the CAD CVT exhibited motion as perceived during the design phase.

Ensuring the stability and alignment of the output disk is important because it rotates inside the circumferentially arranged disks (CADs). In order to maintain the stability of the output shaft and the output disk, especially during gear-changing operations, alignment shaft '15' has been introduced. For reference, see Figure 3. For a better understanding, please see the two assemblies shown in Figure 21i,j.

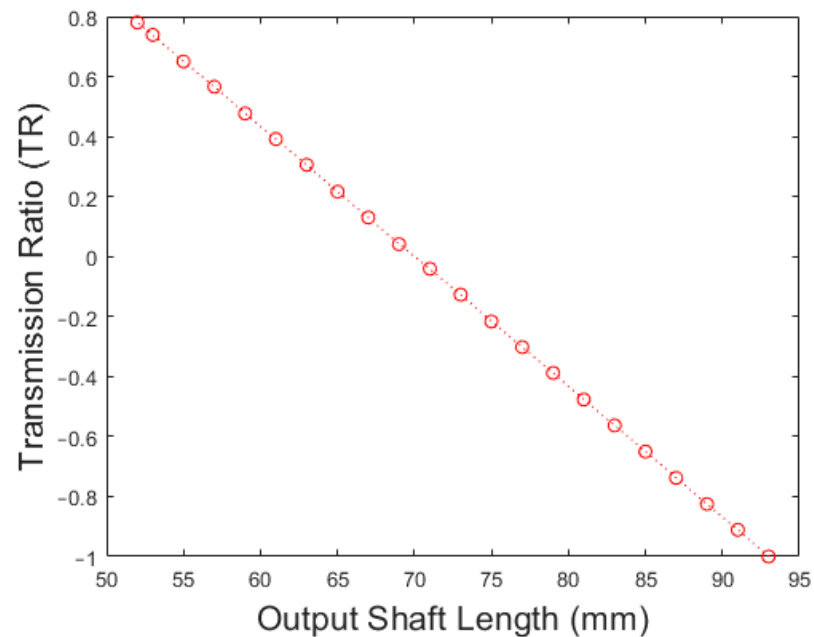


Figure 19. Transmission Ratio vs. Output Shaft Length of Proof of Concept.

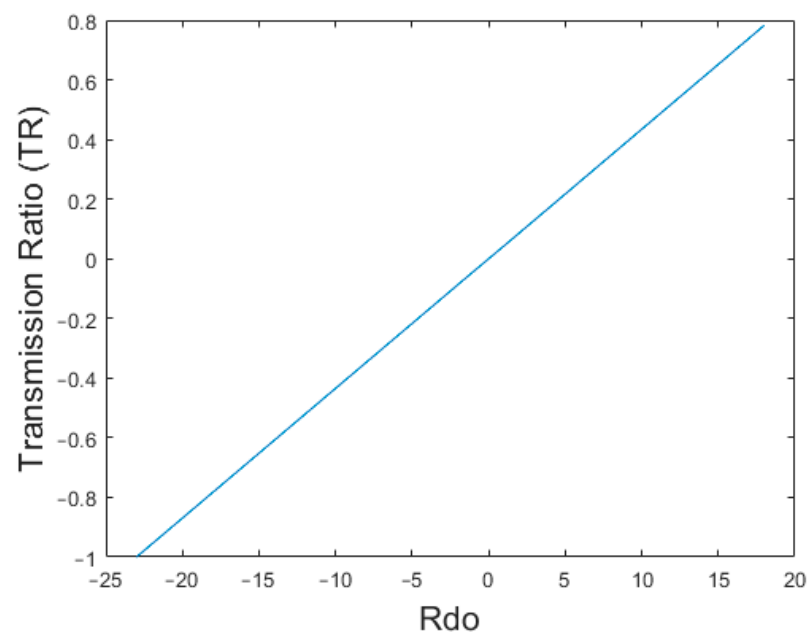


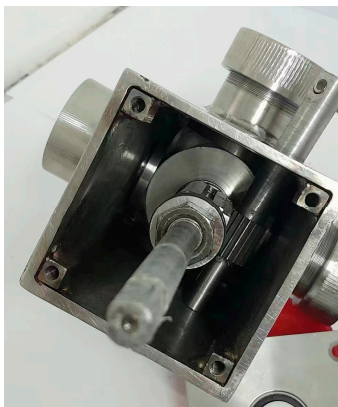
Figure 20. Transmission Ratio vs. Rdo of Proof of Concept (PoC).



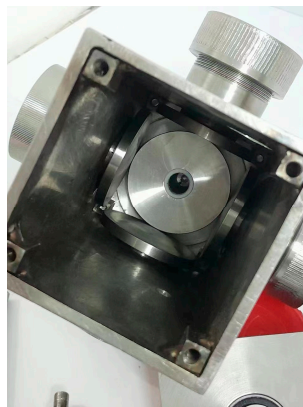
(a)



(b)



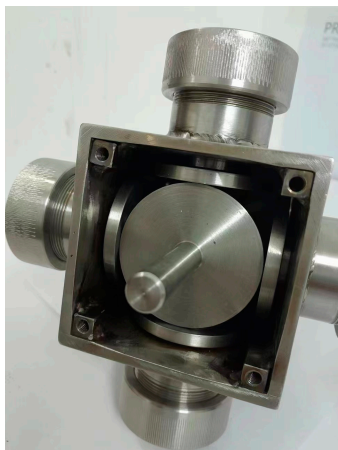
(c)



(d)



(e)



(f)



(g)



(h)

Figure 21. Cont.



(i)



(j)

Figure 21. (a) Experimental setup; (b–h) pictures of CAD CVT Proof of Concept (PoC)/prototype, representing different parts of the CVT for better understanding and visualization. (i,j) Assemblies representing design features incorporated into CAD CVT for improved stability and alignment of output disk and output shaft during normal operation and gear-changing operation.

Table 3. Transmission ratios for different displacements of output shaft of CAD CVT Proof of Concept (PoC).

| S.No | Output Shaft Length. (mm) | R_{do} (mm) | R_{din} (mm) | Transmission Ratio. TR (As per Equation (14)) | Input shaft Rotatio (Degrees) | Output shaft Rotation. (Degrees) | Transmission Ratio. TR (Experimental) |
|------|---------------------------|---------------|----------------|---|-------------------------------|----------------------------------|---------------------------------------|
| 1 | 93 | -23 | 23 | -1 | 360 | -360 | -1 |
| 2 | 91 | -21 | 23 | -0.913 | 360 | -328 | -0.911 |
| 3 | 89 | -19 | 23 | -0.826 | 360 | -297 | -0.825 |
| 4 | 87 | -17 | 23 | -0.739 | 360 | -266 | -0.738 |
| 5 | 85 | -15 | 23 | -0.652 | 360 | -234 | -0.65 |
| 6 | 83 | -13 | 23 | -0.565 | 360 | -203 | -0.563 |
| 7 | 81 | -11 | 23 | -0.478 | 360 | -172 | -0.477 |
| 8 | 79 | -9 | 23 | -0.391 | 360 | -140 | -0.388 |
| 9 | 77 | -7 | 23 | -0.304 | 360 | -109 | -0.302 |
| 10 | 75 | -5 | 23 | -0.217 | 360 | -78 | -0.2166 |
| 11 | 73 | -3 | 23 | -0.130 | 360 | -46 | -0.127 |
| 12 | 71 | -1 | 23 | -0.043 | 360 | -15 | -0.041 |
| 13 | 69 | 1 | 23 | 0.043 | 360 | 15 | 0.041 |
| 14 | 67 | 3 | 23 | 0.130 | 360 | 47 | 0.13 |
| 15 | 65 | 5 | 23 | 0.217 | 360 | 78 | 0.216 |
| 16 | 63 | 7 | 23 | 0.304 | 360 | 110 | 0.3055 |
| 17 | 61 | 9 | 23 | 0.391 | 360 | 141 | 0.3916 |
| 18 | 59 | 11 | 23 | 0.478 | 360 | 172 | 0.477 |
| 19 | 57 | 13 | 23 | 0.565 | 360 | 204 | 0.566 |
| 20 | 55 | 15 | 23 | 0.652 | 360 | 234 | 0.65 |
| 21 | 53 | 17 | 23 | 0.739 | 360 | 266 | 0.7388 |
| 22 | 52 | 19 | 23 | 0.826 | 360 | 281 | 0.78 |

3. Results and Discussion

The most important outcome of the current research is the design of the CAD CVT. The design of the new CVT provides numerous advantages. Some advantages of the CAD CVT are discussed in the following paragraphs. For better visualization and understanding of the design, refer to Figures 1–3. References to commercially important CVTs like the push belt CVT, Toroidal CVT, and Ball-type CVTs (Milner CVT, Nu Vinci CVT, etc.) have been made where necessary.

The new CVT has a simple operation mechanism. The gear ratio is changed by axial sliding of the output shaft with the help of a simple rack-and-pinion mechanism.

An increase in the number of CADs does not increase the complexity of the gear-change mechanism. In other words, irrespective of the number of CADs, the gear-changing mechanism will require only the rack-and-pinion mechanism and the output shaft. In the case of the Toroidal CVT, increasing the number of generatrix increases the complexity of the gear-changing mechanism.

Another important characteristic of the CAD CVT design is that CADs do not require tilting, i.e., the CADs rotate about their own axes; however, the axes of rotation of the CADs are fixed and do not experience any sort of rotation. For comparison, we consider the Toroidal CVT and Ball-type CVT. In the Toroidal CVT, the generatrix not only rotates about its own axis but its axis of rotation is also subjected to tilt in order to achieve gear ratio variation. Similarly, the Ball-type CVT requires both rotation of the balls about its own axis of rotation and tilt of the axis of the rotation of the balls. The additional requirement of tilt in Toroidal and Ball-type CVTs increases the complexity of the gear-changing mechanism.

The CAD CVT experiences one sliding friction contact and one rolling friction contact in series during gear ratio changes, while the Toroidal CVT and the Ball-type CVT experience two sliding friction contacts in series during gear ratio changes.

The CAD CVT can have point contact or line contact, whereas Toroidal CVTs and Ball-type CVTs can only have point contact. Line contact has higher spin losses; however, it provides higher torque capacity as compared to point contact.

Since the frictional contacts between the output disk and CADs can be shifted to either side of the plane containing the axis of rotation of the CADs, directional reversal including a neutral gear ratio is possible without requiring an additional gear set or clutches. Since the aforementioned condition is not possible in the Toroidal CVT, Push belt CVT, and Ball-type CVT, they cannot achieve direction reversal independently.

Equation (14) shows the transmission ratio. Figure 7 shows the corresponding graph. It can be observed that the transmission ratio contains positive, negative, and neutral gear ratios. The CAD CVT can change direction without requiring an additional gear set or clutches. An important observation is that the gear ratio in the CAD varies from -1 to <1 . The gear ratio will always remain less than one because when the output shaft is fully displaced, there comes a point where it touches the input disk. For proper operation of the CVT, there must be some tolerance between the input disk and the output disk. If 'R' is the radius of the CAD, 't' is the thickness of the input and output disk, and 'tol' is the required tolerance between the input and output disks, then the gear ratio range is from $(-1 + (R - (t/2 + tol))/R)$. For the sake of simplicity, we can assume the gear ratio range to be equal to -1 to 1 . If we apply a gear set with gear ratio 'n' at the input shaft of the CAD CVT, then the transmission ratio of the system will become $n*(-1$ to $1)$ or $(-n$ to $n)$. So, we can easily achieve any gear ratio range in the CAD CVT.

Equation (28) shows the torque capacity of the CAD CVT. Figure 9 shows the corresponding graph. It can be observed that torque capacity mainly depends on the amount of axial force applied to the CADs and the number of CADs. The axial load applied to CAD is transferred to the tractive contact between the CAD and the output disk and input disk. The maximum pressure that a material can bear at the point of contact is limited. For example, the maximum pressure in the case of steel-on-steel contact is limited to 2–3 GPa. Therefore, the maximum axial load that we can apply to the CAD is limited. That is why CVTs with a single traction point constraint like DH CVT, Spherical CVT, etc., have low

torque capacity. Since the CAD CVT can have any number of CADs (preferably 3 or more), it can be designed for very high torques.

It is evident from Equations (14) and (28) that the transmission ratio and torque capacity of the CAD CVT are independent of each other. Increasing the torque capacity either by increasing the axial applied force to the CAD or the number of CADs will not affect the transmission ratio range.

Equations (80) and (81) show the frictional losses in the CAD CVT. The main frictional losses in the CAD CVT are (i) spin losses at the traction contact between CADs and the input and output disks; (ii) rolling frictional losses at the traction contact between the CADs and the input disk and output disk; and (iii) frictional losses in the ball bearings, roller bearings, and thrust bearings supporting different elements of the CAD CVT.

Spin losses can be considerably reduced if the line contact between the CADs and the input disk and output disk is changed to point contact. However, it depends on the specific situation. If there is a space constraint and a compact CVT with high torque capacity is required, then we can have line contact at the cost of efficiency.

The manufacturing of a Proof of Concept (POC) consisting of four CADs was intended to verify the basic functionality of the CAD CVT that was perceived during the design synthesis phase. The PoC successfully demonstrated that the CAD CVT can (i) provide a continuum of gear ratios between two points, (ii) achieve directional reversal without requiring an additional gear set and clutches, (iii) achieve a neutral gear ratio without requiring an additional gear set and clutches, and (iv) transmit torque through multiple traction points. The design of an experimental setup that will verify other important parameters of the CVT that are theoretically derived in this research is currently in progress.

4. Conclusions

As per the literature survey, it was observed that all known CVTs require an additional gear set and clutches for direction reversal. However, the Spherical CVT and DH CVT were exceptions, but the problem with the Spherical CVT and DH CVT is that they have a single traction point, which results in low torque capacity. In order to solve this problem, a novel CVT was proposed and named the Circumferentially Arranged Disks CVT (CAD CVT). A Proof of Concept (PoC) of the new CVT with four CADs was manufactured. The PoC successfully demonstrated the basic functionality of the CVT. Analyses of the CAD CVT revealed that it has some major advantages over the commercially available CVTs like the Push Belt CVT and Toroidal CVT. Some of the major advantages are as follows:

- I. The CAD CVT can achieve a reverse gear ratio and a neutral gear ratio without requiring an additional gear set.
- II. The CAD CVT can have any number of CADs.
- III. The CAD CVT can be designed to either have point contact or line contact at its traction points. Point contact can be achieved by changing the contact line at the input and output disks from linear to circular shape. Point contact will provide higher efficiency but lower torque capacity, whereas line contact will provide higher torque capacity but lower efficiency.
- IV. The CAD CVT can be designed for both high-torque and low-torque applications. As per the simulation results shown in Figure 9, a CAD CVT with $n = 10$ CADs can achieve a torque capacity of 572 Nm, and with $n = 20$, it can achieve a torque capacity of 2291 Nm. This is much higher than the commercially available CVTs, i.e., the Push Belt CVT (250 Nm) and Toroidal CVT (450 Nm).
- V. The complexity of the gear-changing mechanism of the CAD CVT is independent of the number of CADs and the number of traction points.

Because of the aforementioned advantages, the new CVT is expected to have a significant impact on high-torque applications, especially trucks and trailers. Moreover, it will have a positive impact on land transport including EVs, robotics, wind turbines, etc. Since this is a new CVT, there is a scope for further analyses and improvements. Work on

analyzing different aspects of the CVT and bringing about further design improvements is in progress.

Author Contributions: Conceptualization, M.B. and Q.Z.; Methodology, M.B. and Q.Z.; Software, A.E. and M.K.N.; Validation, M.B.; Formal Analysis, M.B., Q.Z., S.R.Q. and M.K.N.; Investigation, M.B.; Resources, Q.Z.; Data Curation, M.B., S.R.Q. and M.K.N.; Writing—Original Draft, M.B.; Writing—Review and Editing, A.E. and S.K.; Visualization, M.B.; Supervision, Q.Z.; Project Administration, Q.Z.; Funding Acquisition, Q.Z. All authors have read and agreed to the published version of the manuscript.

Funding: Funding was provided by National Natural Science Foundation of China with project grant no 52171299.

Data Availability Statement: The original contributions presented in the study are included in the article. Further inquiries can be directed to the authors.

Conflicts of Interest: The authors declare no conflict of interest.

References

1. Carbone, G.; Mangialardi, L.; Mantriota, G. A comparison of the performances of full and half toroidal traction drives. *Mech. Mach. Theory* **2004**, *39*, 921–942. [CrossRef]
2. Ruan, J.; Walker, P.D.; Wu, J.; Zhang, N.; Zhang, B. Development of continuously variable transmission and multi-speed dual-clutch transmission for pure electric vehicle. *Adv. Mech. Eng.* **2018**, *10*, 1–15. [CrossRef]
3. Jawad, Q.A.; Ali, A.K. Comparison of CVT Performance with the Manual and Automatic Transmission for Evaluation the Fuel Consumption and Exhaust Emissions. *Basrah J. Eng. Sci.* **2020**, *20*, 15–22. [CrossRef]
4. Nguyen, V.H.; Do, T.C.; Ahn, K.K. Investigation and Optimization of Energy Consumption for Hybrid Hydraulic Excavator with an Innovative Powertrain. *Actuators* **2023**, *12*, 382. [CrossRef]
5. Sheng, Y.; Escobar-Naranjo, D.; Stelson, K.A. Feasibility of Hydrostatic Transmission in Community Wind Turbines. *Actuators* **2023**, *12*, 426. [CrossRef]
6. Cotrell, J. Assessing the Potential of a Mechanical Continuously Variable Transmission for Wind Turbines. WindPower 2005 Denver, Colorado May 15–18, 2005 [Online]. Available online: <http://www.osti.gov/bridge> (accessed on 1 December 2023).
7. Kim, J.; Park, F.C.; Park, Y. Design, analysis and control of a wheeled mobile robot with a nonholonomic spherical CVT. *Int. J. Robot. Res.* **2002**, *21*, 409–426. [CrossRef]
8. Mobedi, E.; Ismet, M.C.D. A Continuously Variable Transmission System Designed for Human-Robot Interfaces. In Proceedings of the Asian Mechanism and Machines Science Conference (Asian MMS), Bengaluru, India, 17–19 December 2018; Springer: Berlin/Heidelberg, Germany, 2018. [CrossRef]
9. Mobedi, E.; Dede, M.I.C. Geometrical analysis of a continuously variable transmission system designed for human-robot interfaces. *Mech. Mach. Theory* **2019**, *140*, 567–585. [CrossRef]
10. Parween, R.; Widanage, K.N.D.; Godaba, H.; Herzig, N.; Li, Y.; Glovnea, R. Design of a Continuous Variable Transmission based Nuclear Decommissioning Robotic Arm. Available online: https://www.robot.t.u-tokyo.ac.jp/Robotics_for_nuclear_environments/Parween.pdf (accessed on 1 December 2023).
11. Chen, X.; Hang, P.; Wang, W.; Li, Y. Design and analysis of a novel wheel type continuously variable transmission. *Mech. Mach. Theory* **2017**, *107*, 13–26. [CrossRef]
12. Kazerounian, K.; Furu-Szekely, Z. Parallel disk continuously variable transmission (PDCVT). *Mech. Mach. Theory* **2006**, *41*, 537–566. [CrossRef]
13. Komatsubara, H.; Kuribayashi, S. Research and development of cone to cone type CVT (1st Report, Fundamental structure, speed change mechanism and design of CTC-CVT). *Trans. JSME* **2017**, *83*, 16–00477. [CrossRef]
14. Carter, J.; Miller, D. *The Design and Analysis of an Alternative Traction Drive CVT*; SAE Technical Paper 2003-01-0970; SAE: Warrendale, PA, USA, 2003. [CrossRef]
15. Shen, C.J.; Yuan, S.H.; Hu, J.B.; Wu, W.; Wei, C.; Chen, X. Principle and characteristics of original hydraulic traction drive CVT. *J. Cent. South Univ.* **2014**, *21*, 1654–1659. [CrossRef]
16. Ghariblu, H.; Behroozirad, A.; Madandar, A. Traction and Efficiency Performance of Ball Type CVTs. 2014. [Online]. Available online: <http://www.iust.ac.ir> (accessed on 1 December 2023).
17. Li, Q.; Li, H.; Yu, D.; Yao, J. A novel continuously variable transmission with logarithmic disc generatrix. *Mech. Mach. Theory* **2015**, *93*, 147–162. [CrossRef]
18. Li, C.; Li, H.; Li, Q.; Zhang, S.; Yao, J. Modeling, kinematics and traction performance of no-spin mechanism based on roller-disk type of traction drive continuously variable transmission. *Mech. Mach. Theory* **2019**, *133*, 278–294. [CrossRef]
19. Li, C.; Yao, J.; Li, H.; Fu, L. Research on a novel configuration synthesis method of no-spin traction continuously variable transmission. *Mech. Mach. Theory* **2020**, *152*, 103963. [CrossRef]

20. Delkhosh, M.; Foumani, M.S. Multi-Objective Geometrical Optimization of Full Toroidal CVT. *Int. J. Automot. Technol.* **2013**, *14*, 707–715.
21. Tomaselli, M.; Bottiglione, F.; Lino, P.; Carbone, G. NuVinci drive: Modeling and performance analysis. *Mech. Mach. Theory* **2020**, *150*, 103877. [[CrossRef](#)]
22. Verbelen, F.; Derammelaere, S.; Sergeant, P.; Stockman, K. Half toroidal continuously variable transmission: Trade-off between dynamics of ratio variation and efficiency. *Mech. Mach. Theory* **2017**, *107*, 183–196. [[CrossRef](#)]
23. Wong, P.K.; Xie, Z.; Chen, Y. An Experimental Study on Dynamics of a Novel Dual-Belt Continuous Variable Transmission Based on a Newly Developed Test Rig. *Shock. Vib.* **2015**, *2015*, 857978. [[CrossRef](#)]
24. Narita, K.; Priest, M. Metal-metal friction characteristics and the transmission efficiency of a metal V-belt-type continuously variable transmission. *Proc. Inst. Mech. Eng. Part J J. Eng. Tribol.* **2007**, *221*, 11–26. [[CrossRef](#)]
25. P. K.P., J. K.M., P. B.S.; Maluk, P. Cam Based IVT. Available online: www.iosrjournals.org (accessed on 1 December 2023).
26. Olyaei, A. Novel continuously variable transmission mechanism. *SN Appl. Sci.* **2019**, *1*, 1032. [[CrossRef](#)]
27. Micklem, J.D.; Longmore, D.K.; Burrows, C.R. Modelling of the steel pushing V-belt continuously variable transmission. *Proc. Inst. Mech. Eng. Part C J. Mech. Eng. Sci.* **1994**, *208*, 13–27. [[CrossRef](#)]
28. Lin, X.; Peng, Y.; Hong, R.; Wang, Y. Research on a novel discrete adjustable radiuses type continuously variable transmission. *Meccanica* **2022**, *57*, 1155–1171. [[CrossRef](#)]
29. Dresscher, D.; Naves, M.; De Vries, T.J.A.; Buijze, M.; Stramigioli, S. Power split based Dual Hemispherical Continuously Variable Transmission. *Actuators* **2017**, *6*, 15. [[CrossRef](#)]
30. Kim, J.; Park, F.C.; Park, Y.; Shizuo, M. Design and analysis of a spherical continuously variable transmission. *J. Mech. Des.* **2002**, *124*, 21–29. [[CrossRef](#)]
31. Budynas, R.G.; Nisbett, J.K. *Shigley's Mechanical Engineering Design*, 9th ed.; Cylindrical Contact, Equation (3–73) and Equation (3–74); McGraw-Hill: New York, NY, USA, 2011; p. 125.

Disclaimer/Publisher's Note: The statements, opinions and data contained in all publications are solely those of the individual author(s) and contributor(s) and not of MDPI and/or the editor(s). MDPI and/or the editor(s) disclaim responsibility for any injury to people or property resulting from any ideas, methods, instructions or products referred to in the content.